Journal Pre-proof

One-step silver coating of polypropylene surgical mask with antibacterial and antiviral properties

Ivan Vito Ferrari, Giulia Giuntoli, Anissa Pisani, Aida Cavallo, Paola Mazzetti, Rossella Fonnesu, Alfredo Rosellini, Mauro Pistello, Tamer Al Kayal, Antonino Cataldo, Roberto Montanari, Alessandra Varone, Micaela Castellino, Simonetta Antonaroli, Giorgio Soldani, Paola Losi

Please cite this article as: , One-step silver coating of polypropylene surgical mask with antibacterial and antiviral properties, *HELIYON* (2024), doi: https://doi.org/10.1016/j.heliyon.2023.e23196.

This is a PDF file of an article that has undergone enhancements after acceptance, such as the addition of a cover page and metadata, and formatting for readability, but it is not yet the definitive version of record. This version will undergo additional copyediting, typesetting and review before it is published in its final form, but we are providing this version to give early visibility of the article. Please note that, during the production process, errors may be discovered which could affect the content, and all legal disclaimers that apply to the journal pertain.
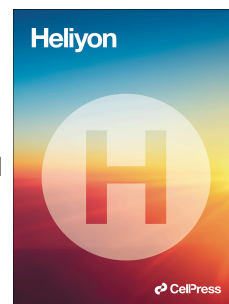
Manuscript

One-step silver coating of polypropylene surgical mask with antibacterial and antiviral properties

Ivan Vito Ferrari[1][§][*], Giulia Giuntoli[1][§], Anissa Pisani[1], Aida Cavallo[1], Paola Mazzetti[2], Rossella Fonnesu[2], Alfredo Rosellini[2], Mauro Pistello[2], Tamer Al Kayal[1], Antonino Cataldo[3], Roberto Montanari[4], Alessandra Varone[4], Micaela Castellino[5], Simonetta Antonaroli[6], Giorgio Soldani[1] and Paola Losi[1]

[1]Institute of Clinical Physiology, National Research Council, Massa, 54100, Italy

[2]Virology Unit, Pisa University Hospital, Pisa, Italy and Retrovirus Center, Department of Translational Research and New Technologies in Medicine and Surgery, University of Pisa, Pisa, 56126, Italy

[3]ENEA, Casaccia Research Centre, Rome, 00123, Italy

[4] Department of Industrial Engineering, University of Rome Tor Vergata, Rome, 00133, Italy

[5]Department of Applied Science and Technology, Politecnico di Torino, 10129, Turin, Italy

[6]Department of Chemical Sciences and Technology, University of Rome Tor Vergata, Rome, 00133, Italy

Ivan Vito Ferrari ivanvitoferrari@ifc.cnr.it

Giulia Giuntoli giuntoli.g@ifc.cnr.it

Anissa Pisani apisani@ifc.cnr.it

Aida Cavallo aida.cavallo@ifc.cnr.it

Paola Mazzetti paola.mazzetti@unipi.it

Rossella Fonnesu fonnesurossella@gmail.com

Alfredo Rosellini al.rosellini@ao-pisa.toscana.it

Mauro Pistello mauro.pistello@unipi.it

Tamer Al Kayal atamer@ifc.cnr.it

Antonino Cataldo antonino.cataldo@enea.it

Roberto Montanari roberto.montanari@uniroma2.it

Alessandra Varone alesssandra.varone@uniroma2.it

Micaela Castellino micaela.castellino@polito.it

Simonetta Antonaroli simonetta.antonaroli@uniroma2.it

Giorgio Soldani giorgio.soldani@ifc.cnr.it

Paola Losi losi@ifc.cnr.it

§These authors contributed equally to this work

*Corresponding author: Ivan Vito Ferrari ivanvitoferrari@ifc.cnr.it

Abstract

Face masks can filter droplets containing viruses and bacteria minimizing the transmission and spread of respiratory pathogens but are also an indirect source of microbes transmission.

A novel antibacterial and antiviral Ag-coated polypropylene surgical mask obtained through the *in situ* and one-step deposition of metallic silver nanoparticles, synthesized by silver mirror reaction combined with sonication or agitation methods, is proposed in this study.

SEM analysis shows Ag nanoparticles fused together in a continuous and dense layer for the coating obtained by sonication, whereas individual Ag nanoparticles around 150 nm were obtained combining the silver mirror reaction with agitation. EDX, XRD and XPS confirm the presence of metallic Ag in both coatings and also oxidized Ag in samples by agitation. A higher amount of Ag nanoparticles is deposited on samples by sonication, as calculated by TGA. Further, both coatings are biocompatible and show antibacterial properties: coating by sonication caused 24% and 40% of bacterial reduction while coating by agitation 48% and 96% against *S. aureus* and *E. coli,* respectively. At 1 minute of contact with SARS-CoV-2, the coating by agitation has an antiviral capacity of 75% against 24% of the one by sonication. At 1 h, both coatings achieve 100% of viral inhibition. Nonetheless, larger samples could be produced only through the silver mirror reaction combined with agitation, preserving the integrity of the mask.

In conclusion, the silver-coated mask produced by silver mirror reaction combined with agitation is scalable, has excellent physico-chemical characteristics as well as significant biological properties, with higher antimicrobial activities, providing additional protection and preventing the indirect transmission of pathogens.

Keywords

Silver mirror reaction; silver coating; surgical masks; antimicrobial properties.

1 Introduction

The recent COVID-19 pandemic has highlighted that emerging and unexpected pathogenic agents can disrupt and upset the lives of billions of people, if without adequate protection. The use of face masks, especially in closed places with poor ventilation, has been demonstrated to greatly minimize the transmission and spread of SARS-CoV-2 [1][2][3]. Surgical masks are primarily used by healthcare workers to decrease exposure to aerosols and droplets, preventing infections, and have been the most used personal protective equipment after the COVID-19 pandemic outbreak [2][3]. Commonly, surgical masks are made of polypropylene (PP), polystyrene, polycarbonate, or polyester and their filtration efficacy depends on the number, type and structure of the overlapped layers [2][4][5]. The majority of surgical masks consist of three/four layers of non-woven fabric, with a spunbond-meltblown-spunbond stacked structure that hinders the transmission of small particles and pathogens. Each layer has a different function: the innermost layer absorbs moisture, the middle layer works as a filter, and the outermost hydrophobic layer repels respiratory droplets [2][5]. The non-woven fabric structure confers excellent barrier properties arising from unique porous networks, which also guarantee good breathability [5]. However, the filtration efficiency dramatically declines in a few hours [6][7].

Novel technologies have been recently applied to improve surgical masks performances, by adding antibacterial, antiviral, super hydrophobic, or self-cleaning/self-disinfecting functionalities. These advanced masks are expected to be more efficient, durable, and environmentally friendly [7][8][9][10][11]. Metal nanoparticles (NPs) of silver [12][13][14][15][16], copper [17][18][19], zinc oxide [17][20], and others, are known for their antimicrobial properties, derived from their size, shape, surface charge, functionality and composition. Among them, silver nanoparticles (AgNPs) have a wide range of applications in biomedicine and are exploited for their broad-spectrum antimicrobial, antioxidant, anti-inflammatory, and wound healing properties [12][21][22]. The antiviral activity of AgNPs was reported against several viral strains, such as influenza, HIV, hepatitis B, and SARS-CoV-2 [11][15][17][23]. Moreover, AgNPs have long-term stability and are suited for high-scale production [24].

Fabrics functionalized with AgNPs have strong antibacterial activity against both gram-negative and gram-positive bacteria [16][25]. Natural fabrics have been functionalized by the *in situ* incorporation of AgNPs into the fabric matrix, obtaining multifunctional textiles with long-term antibacterial and UV-protection properties, even after several washing cycles [16]. In hospital environments, these textiles can prevent or minimize pathogens infections. The addition of AgNPs to surgical masks enhances their antimicrobial action through different mechanisms, other than their inherent filtration properties [4][5][7][21][23][26]. Surgical masks coated with colloidal AgNPs by direct soaking

demonstrated antibacterial activity against either *S. aureus* or *E. coli*, with respect to the untreated mask [21]. Baselga et al. presented a virucidal coating based on AgNPs and polyethyleneimine on face masks and other polymeric substrates. Their results indicate a very high efficacy, with a viral load reduction of 99.99% against SARS-CoV-2 virus after 2 h of infection [23].

In this study, a novel antibacterial and antiviral Ag-coating on surgical mask was developed through the *in situ* deposition of metallic AgNPs on the spunbond PP layer of the mask. Herein, the chemical method selected for the coating is the Silver Mirror Reaction (SMR), also known as "Tollens' Test", a redox reaction commonly used to detect the presence of aldehydes or ketones in alkaline ammoniacal silver solutions [27][28]. Historically, the SMR has been also employed as an efficient coating method for the deposition of thin films of silver nanoparticles on glass [29][30], however other organic and inorganic surfaces have been coated [29][31][32]. For instance, the SMR has been used on PP substrates, after surface's sensitization with $SnCl_2$ [32][33], surface activation by plasma treatments [34], UV-assisted implantation of functional groups [35], or the use of precoatings such as polyethyleneimine [23], poly-dopamine [36], or poly-acrylonitrile [37].

The novelty of our study, compared to others, is that the formation and deposition of AgNPs during the SMR process occurs directly on the surface of PP microfibers without intermediates. Ag-coatings using the SMR were investigated, evaluating the coatings' homogeneity, performing the physico-chemical characterization and assessing the biocompatibility, the antibacterial activity against *S. aureus* and *E. coli*, and the antiviral properties against SARS-CoV-2.

2   Materials and Methods

2.1   Chemical Reactants

Cetyltrimethylammonium bromide (CTAB, MW 364.45 g mol^{-1}), silver nitrate crystals ($AgNO_3$, MW 169.87 g mol^{-1}), ammonium hydroxide (NH_4OH, 28.0-30.0% v/v), D-(+)-glucose (MW 180.16 g mol^{-1}) and sodium hydroxide (NaOH, MW 40.00 g mol^{-1}) were purchased from Merck KGaA (Darmstadt, Germany). All reagents were used without further purification. Deionized water (dH$_2$O, Dia Class 120, Quality Invents s.r.l., Milan, Italy) was obtained via a reverse osmosis process.

Mouse fibroblasts L929 (ICLC ATL95001) were purchased from Biobanking and Cell Factory Hospital San Martino (Genova, Italy); human keratinocytes HaCaT (BS CL 168) were purchased from Biobanking of Veterinary Resources, Istituto Zooprofilattico Sperimentale della Lombardia e dell'Emilia Romagna (Brescia, Italy). *Escherichia coli* and *Staphylococcus aureus* were purchased from Thermo Fisher Scientific (Milan, Italy).

2.2   Silver Mirror Reaction (SMR) on surgical face masks

Each specimen (1 x 1.5 cm) of the outer spunbond layer of PP surgical masks was immersed in a solution of 1mM CTAB for at least 1 minute to increase the PP wettability. Then, the SMR was performed by submerging the specimens in the SMR solution obtained by adding in order the following reagents: 0.6 mL of 0.2 M silver nitrate $AgNO_3$, 0.1 mL of 28-30% NH_4OH, 1 mL of 0.2 M glucose, and 0.1 mL of 1M NaOH. The final $AgNO_3$ concentration is 66.7 mM.

The SMR was combined with two techniques, specifically:

1) *Sonication.* The SMR reaction was carried out in an ultrasonic bath (Labsonic LBS2, Falc Instruments s.r.l., Treviglio, Italy) at 40 °C for 10 min in dark conditions, with the following parameters: frequency 59 kHz, power 100%, temperature 40 °C. Finally, samples were washed with dH_2O and dried at room temperature. Samples coated with the SMR and sonication are indicated as Ag-1.

2) *Agitation.* The SMR reaction was carried out under continuous agitation in a horizontal shaker (ASAL VDRL 711D, Milan, Italy) at 40 rpm and 37 °C for 40 min. Finally, samples were washed and dried as above. Samples coated with the SMR and agitation are indicated as Ag-2.

2.3   Morphological analysis

Morphological investigations were performed by stereo microscopy (Axio Zoom V16 equipped with a digital camera AxioCam 506 Mono, Carl Zeiss, Oberkochen, Germany) at different magnifications, and by scanning electron microscopy (SEM, FlexSEM 1000, Hitachi, Tokyo, Japan). ImageJ 1.52 software (Wayne Rasband, National Institutes of Health, Bethesda, MD, USA) was used to estimate the silver nanoparticles size on silver-coated PP fibers.

2.4   Physico-chemical characterization

The sessile drop method was employed to evaluate the static water contact angle (WCA). A 3 µL drop of dH_2O was deposited at room temperature on the surface of samples using a micropipette. ImageJ 1.52 was used to measure the contact angles from digital images. The average WCA was calculated by measuring at least 6 drops on each sample.

SEM with Energy Dispersive X-ray Spectroscopy detector (SEM-EDX, FEI Quanta 450 ESEM-FEG, FEI Europe BV, Eindhoven, The Netherlands) was used to assess the surface chemical composition of samples.

Fourier-transform infrared spectroscopy (FTIR) spectra in transmission mode were recorded in the range of 4000–400 cm^{-1} (Spectrum 100, Perkin Elmer, Massachusetts, United States).

X-ray diffraction (XRD) spectra were recorded in the 2Θ angular range at $10-55°$ by using Mo–Kα radiation ($\lambda = 0.709$ Å) with 2Θ angular steps of $0.05°$ and counting time of 2 s per step (Philips PW 1729 diffractometer, Eindhoven, The Netherlands). The phases have been identified by using the JCPDS-ICDD database (Newtown Square, PA 19073, USA) [38].

X-ray photoelectron spectroscopy (XPS) was carried out by means of a PHI Versaprobe 5000 spectrometer, equipped with an Al K-alpha monochromatic line (1486.6 eV), and by using a double charging neutralization procedure, made up by Ar$^+$ and an electron beam, to compensate surface charging phenomena for non-conductive materials. Survey scans have been acquired prior to High Resolution (HR) spectra, in order to check for all the elements present on top of the materials. Both survey and HR measurements have been collected using a 100 µm size diameter analysis spot. Deconvolution procedures on HR spectra have been carried out by using Casa XPS Software (version 2.3.18).

High-resolution Thermogravimetric Analysis (TGA) was conducted under air flux between 30 and 700 °C, by a TA Q500 apparatus with Pt sample holders. The samples (7-9 mg) were heated with a maximum heating rate of 3 K/min using a high-resolution ramp.

2.5 *In vitro biocompatibility assessment*

To evaluate the possible cytotoxic effects of silver-coated masks, the indirect contact assay was conducted according to ISO 10993-5 on L929 mouse fibroblasts and HaCaT human keratinocytes cells as previously reported by Briganti et al. [39].

Briefly, L929 and HaCaT cells were routinely cultured in RPMI 1640 with 10% Fetal Bovine Serum (FBS), 1% L-Glutamine, and 1% streptomycin-penicillin at 37 °C and 5% CO_2.

Cells were seeded in 96 well plates at 1×10^4 cells/well and 2×10^4 cells/well for L929 and HaCaT, respectively. Samples were UV-sterilized for 1 h per side, incubated in cell culture medium (3 cm^2/mL) for 24 h at 37 °C under agitation, then these conditioned media (200 µL/well) were used to treat cells. After 24 h, the cell viability was evaluated by the MTT [3-(4,5 dimethylthiazol-2-yl)-2,5-diphenyl tetrazolium bromide] assay (Merck KGaA), accordingly to the manufacturer protocol. A microplate reader (Spectrafluor Plus; TECAN Austria GmbH, Grödig, Austria) was used to measure the optical density (OD) at 550 nm wavelength. Cells treated with incubated complete medium without samples (blank) were considered as reference and their viability was assumed 100%. At least three independent samples were used for each analysis.

2.6 *Antibacterial activity assessment*

Escherichia coli (Gram-negative) and *Staphylococcus aureus* (Gram-positive) bacteria were chosen to investigate the antimicrobial efficacy of the developed silver-coated surgical mask according to the work by Zheng, et al [12].

E. coli and *S. aureus* were cultured in Mueller-Hinton broth at 37 °C. By ABS measurement at 550 nm, 50 colony forming units (CFU) in 75 µL of *E. coli* or *S. aureus* were estimated and inoculated on round samples (diameter of 8 mm), previously UV-sterilized for 1 h per side. After 2 h, bacteria were plated on Mueller-Hinton agar. The number of CFU was determined after 24 h of incubation at 37 °C, and normalized on the CFU control sample (pristine PP surgical mask) assumed as 100% of bacteria viability.

2.7   *Antiviral properties assessment against SARS-CoV-2*

The antiviral properties of samples (14 mm of diameter), UV-sterilized for 1 h per side, were evaluated against SARS-CoV-2, as previously reported [40][41].

The inactivation percentages of the virus were evaluated after 1, 5, 10, 30 and 60 minutes of contact. The results, expressed as % inhibition of viral growth, were normalized on infected and untreated african green monkey kidney cells (VERO E6) control.

2.8   *Scalability*

The two SMR coating reactions were also applied to real-sized samples, about 15 x 12 cm, to investigate the scalability of the proposed methods. The SMR was performed in a plastic container with either sonication or agitation methods, maintaining the same ratio between SMR solution volume and sample surface used for small specimens. Briefly, samples were first immersed in CTAB, then submerged in the SMR solution obtained by adding in order the following reagents: 74.4 ml of 0.2 M $AgNO_3$, 12.4 ml of 28-30% NH_4OH, 124 ml of 0.2 M glucose, and 12.4 ml of 1M NaOH. The final $AgNO_3$ concentration is 66.7 mM.

2.8.1   *Mechanical characterization*

Samples were subjected to uniaxial tensile test at break with the Zwick-Roell Z1.0 testing machine (ZwickRoell GmbH, Ulm, Germany), equipped with a 100 N load cell. Rectangular specimens (width 25 mm, gauge length 130 mm) were tested at a crosshead speed of 100 mm/min. The thickness was measured before testing with a digital micrometer (MDC-Lite, resolution 0.001 mm, Mitutoyo America Corporation, Illinois, United States) in the central part of the specimens and equaled to 240 µm. Failure was set at a 5% reduction of the maximum stress. Data were normalized and used to

calculate the mechanical properties. The elastic modulus was evaluated from the linear tract of the stress-strains curves between 1 - 2% strain ($R^2 > 0.99$).

2.8.2 Functional tests of Personal Protective Equipment

Bacterial filtration efficiency (BFE) and breathability (or differential pressure test) (Pa/cm^2) were evaluated following UNI EN 14683:2019. The BFE test was conducted by the certified laboratory BioRicerche s.r.l. (Grosseto, Italy).

The breathability test was carried out using Bulldog Plus-R (XEARPRO, Cogliate, Italy). The differential pressure was calculated using the following formula (1):

$$\Delta P = \frac{Xm_1 - Xm_2}{4.9} \tag{1}$$

where Xm_1 is the pressure in Pa measured by the pressure gauge at bottom side of the sample, Xm_2 is the pressure in Pa measured by the pressure gauge at top side of the sample, and 4.9 is the area in cm^2 of the tested sample.

2.9 Statistical analysis

Data are given as mean ± standard deviation (SD). One-way or two-way analysis of variance (ANOVA) was used for comparing data, and p value < 0.05 was considered statistically significant.

3 Results and discussion

3.1 Silver coating on surgical masks

The Ag-1 coating on the surgical face mask was obtained by combining the SMR with the sonication technique and allowed the deposition of a uniform golden coating (Fig. 1b) on the outer spunbond PP layer (Fig. 1a); the Ag-2 coating obtained by combining the SMR with agitation was also uniform and of grey color (Fig. 1c). The aim of this study was to develop an antiviral and antibacterial silver coating on non-woven PP surgical face masks with a one-step process. To allow NPs deposition onto inert polymeric materials, such as PP, a pre-activation of the substrate is typically required to increase its chemical reactivity. PP surface can be activated by wet chemical treatments (e.g., grafting, pad-dry cure, impregnation, etc.) or physical techniques (γ-radiation, UV treatments, plasma treatments) [42]. However, there are major drawbacks derived from these processes: wet treatments usually require a large amount of chemicals and have high waste generation, while physical techniques are usually not energy-efficient and the investment costs are significant. Instead, in this study, the surface tension of PP was reduced by the CTAB surfactant, which is an inexpensive activation method that

does not require specific technologies. Then, the silver coating was obtained directly on the spundbond PP layer of surgical masks through the *in situ* formation and deposition of AgNPs on PP fibers by the Silver Mirror Reaction (SI, Silver Mirror Reaction) [27][28] combined with two different techniques, sonication and agitation.
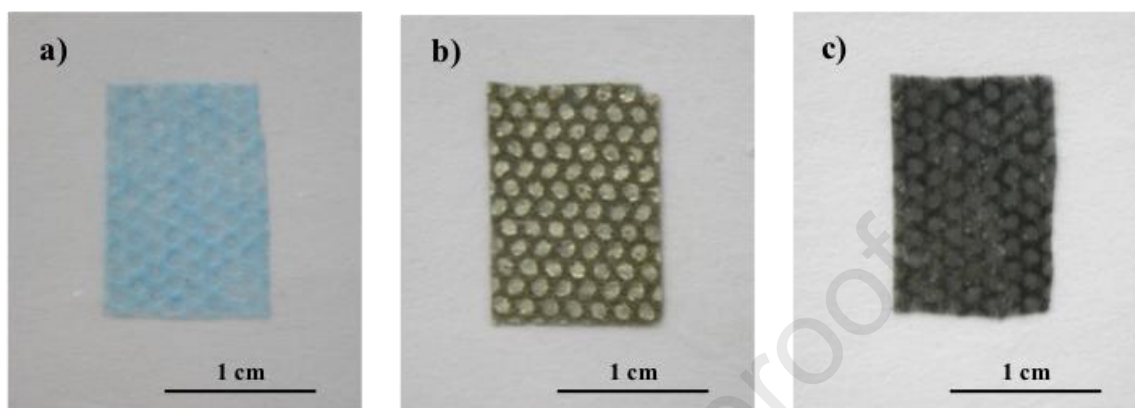

Figure 1. (a) Pristine spunbond polypropylene surgical mask, and silver-coated masks by *in situ* silver mirror reaction (SMR) combined with (b) sonication or (c) agitation methods; scale bar 1 cm.

3.2 Morphological analysis

Pristine, Ag-1, and Ag-2 masks were observed by stereomicroscopy for a qualitative evaluation of the 3D structure of PP fibers (Fig. 2a, c, f) and the silver coating, while SEM microscopy was used to further analyze the coating at the level of individual PP microfibers (Fig. 2b, d, g).

The images captured by stereomicroscopy of Ag-1 (Fig. 2c) and Ag-2 (Fig. 2f) show that PP fibers, as well as welding points, were completely covered by the silver coating. SEM analysis confirmed that the SMR allows the *in situ* chemical synthesis and deposition of AgNPs directly on the PP fibers during their nucleation phase, while the silver mirror forms on the internal side of the vessel. Specifically, on Ag-1 the coating appears continuous and dense, and the AgNPs formed are fused together and not distinguishable separately (Fig. 2d, e). This was probably related to an excessive and uncontrolled growth during the nucleation phase of the AgNPs produced by SMR and sonication method. On the contrary, Ag-2 presented a more homogenous silver coating with smaller AgNPs with an average diameter of about 150 nm (Fig. S1, Supporting Information) and an irregular morphology (Fig. 2g, h). Several clusters randomly distributed on the fibers were also observed in both samples.
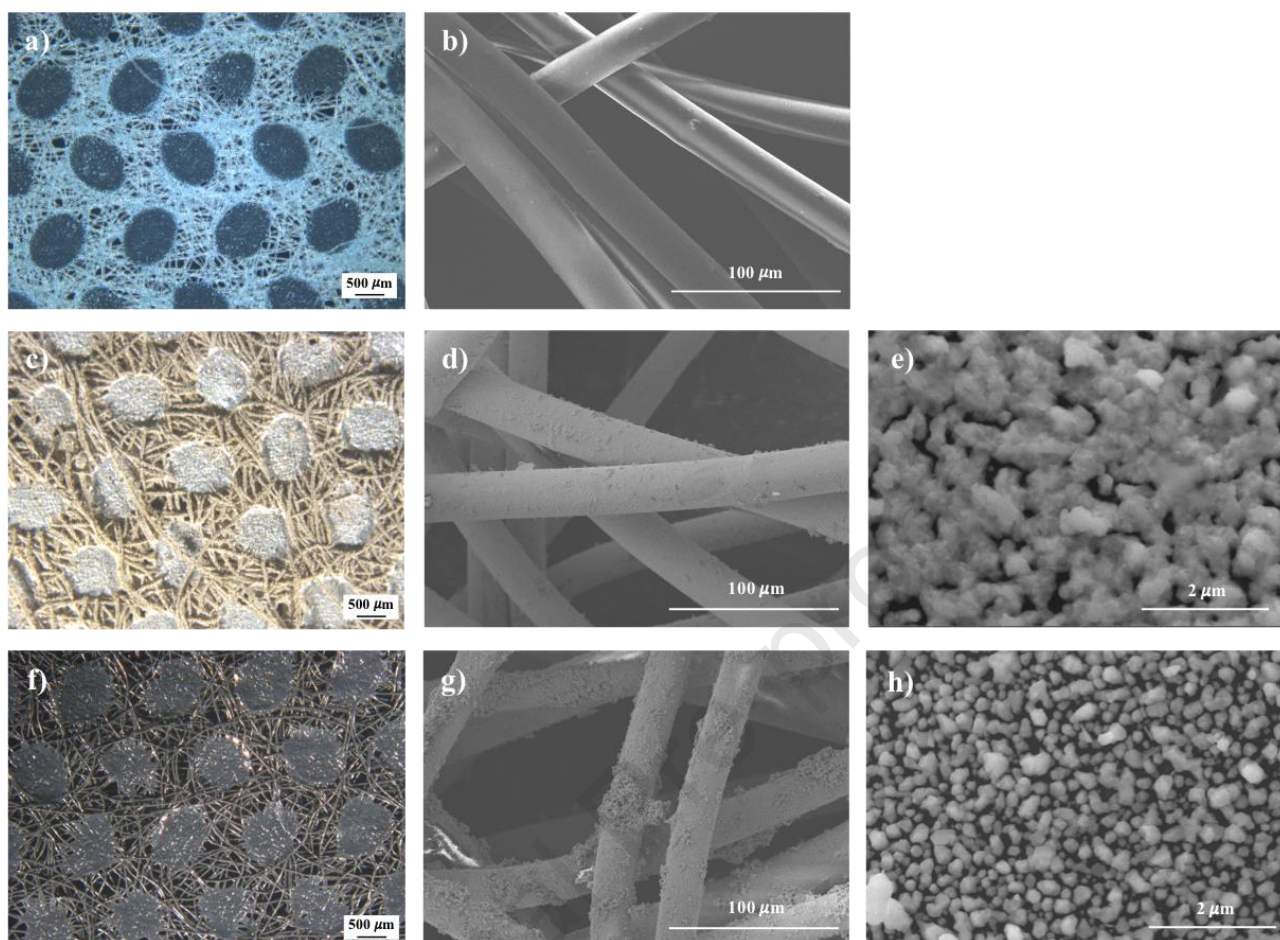
Figure 2. Morphological characterization by stereomicroscopy (left) and SEM imaging (middle and right) at different magnifications of the pristine or Ag-coated outer spunbond layer of polypropylene face masks. (a, b) Pristine layer; (c, d, e) Ag-1 samples, coated by the sonication method; (f, g, h) Ag-2 samples, coated by the agitation method. In stereomicroscopy images, egg-shaped welding points are also visible. Scale bars equal to 500 µm (a, c, f), 100 µm (b, d, g), or 2 µm (e, h).

3.3   Physico-chemical characterization

3.3.1   Wettability

WCA measurements were conducted to verify that the barrier properties of the outer layer of the face mask were preserved. As reported by others [26][43], the pristine spunbond PP layer has a hydrophobic behaviour with a WCA of $116 \pm 4°$; after the coating processes, Ag-1 and Ag-2 have only slightly lower WCA, equal to $104 \pm 7°$ and $107 \pm 4°$, respectively. This demonstrates that the presence of both Ag coatings does not affect the ability of the mask to repel infectious droplets.

3.3.2   SEM-EDX analysis

SEM-EDX analysis was conducted to evaluate the elemental composition of the coatings. The analysis showed a high signal at approximately 0.25 keV and two distinct peaks at around 3.0 keV and 3.2 keV, confirming the pure crystalline character of the metallic AgNPs for both Ag-1 (Fig. 3a,

b) and Ag-2 coatings (Fig. 3c, d). The intensities of the peaks of Ag-1 are higher compared to Ag-2, indicating that more Ag is deposited on PP microfibers by the SMR along with sonication.
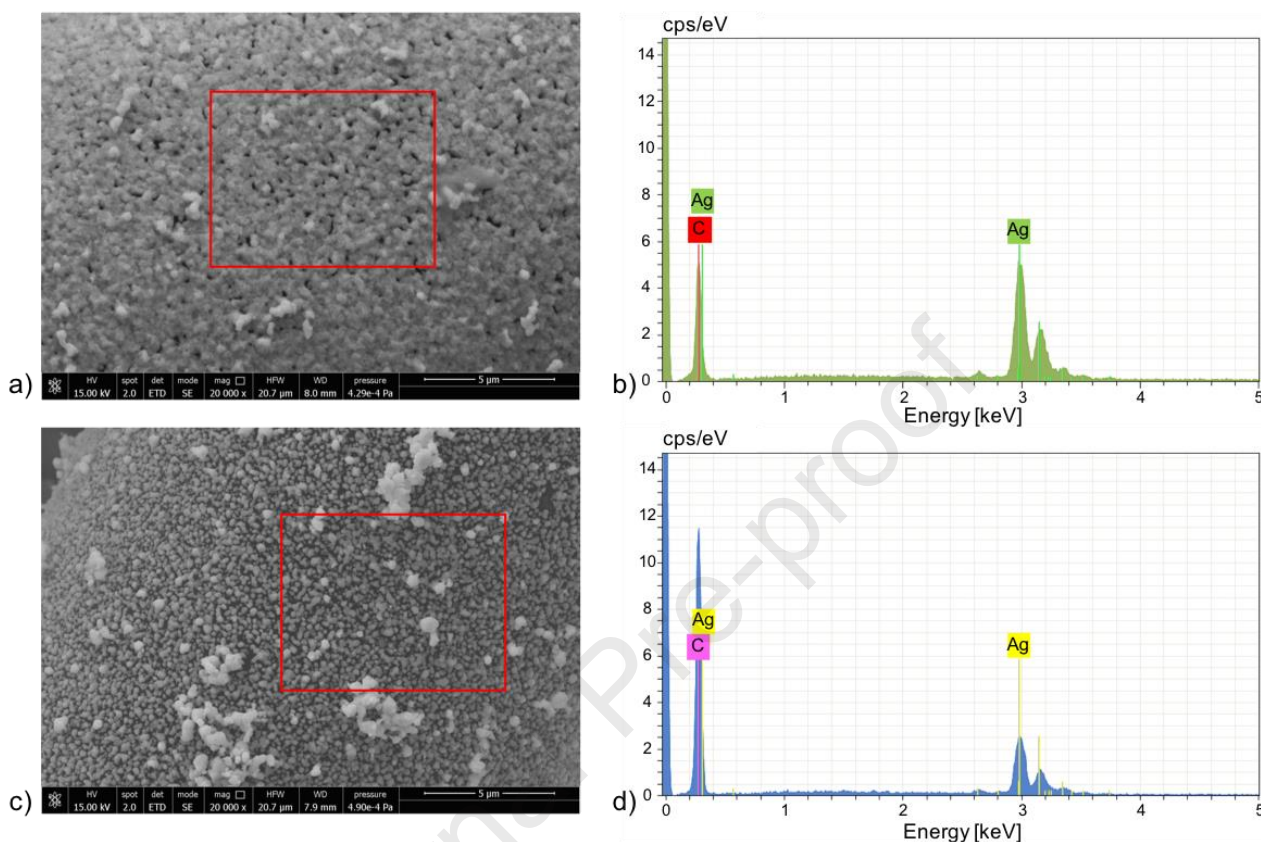

Figure 3. SEM-EDX analysis of (a, b) Ag-1 and (c, d) Ag-2 samples. The red squares represent the area of analysis. Scale bar equal to 5 µm.

3.3.3 FTIR analysis

The FTIR spectra of Ag-1 and Ag-2 were comparable to that of pristine PP since no appreciable variations were observed [44], indicating that no covalent bonds or molecular complexes formed between AgNPs and the underlying PP (Fig. S2, Supporting Information). This suggests that the silver coating obtained by the SMR, for both methods, probably occurs by physical adsorption rather than by chemical bonding.

3.3.4 XRD analysis

Figure 4a shows the XRD spectra of Ag-1 and Ag-2. For comparison, the spectrum of a pristine PP surgical mask is also reported. The XRD spectra display the peaks of Ag (JCPDS-ICDD database file 4-783), demonstrating the presence of metallic AgNPs, with a face-centered cubic structure [44], on PP microfibers for both samples. In particular, Ag-1 shows all the Ag reflections while only (111),

(200), (220) and (311) peaks were visible in Ag-2. These results confirm the presence of AgNPs in both masks and a lower AgNPs amount in Ag-2 where only the first four reflections of Ag could be detected.
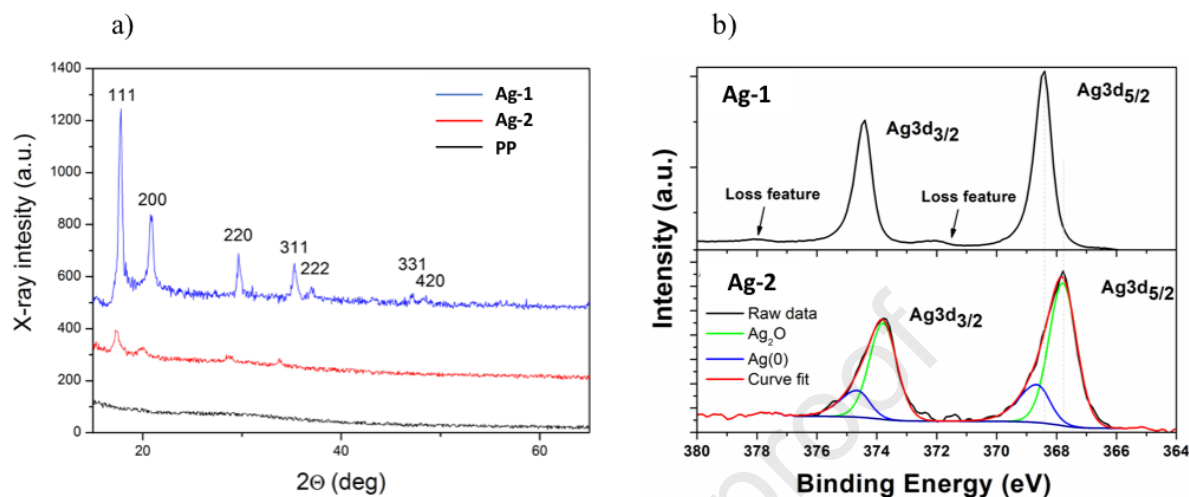

Figure 4. (a) XRD spectra and (b) XPS analysis of pristine spunbond PP surgical mask, Ag-1 and Ag-2 silver-coated masks.

3.3.5 XPS analysis

XPS analysis has been conducted in order to shed light onto AgNPs' surface chemical composition, since their interaction with biological species is led, not only by their size and shape, but also by their surface chemistry (Fig. 4b). Survey scans have been recorded for both Ag-1 and Ag-2 samples (graphs not shown) highlighting the presence of C, O and Ag. No N1s signal has been detected in both samples, which suggests that the Ag precursor ($AgNO_3$) has been completely decomposed during the two deposition reactions. C1s, O1s, Ag3d and AgMNN1 HR regions have been acquired, not only to analyze the Ag oxidation state, but also to calculate the relative atomic concentration of all the elements present on samples surfaces.

The following results were obtained for Ag-1 and Ag-2: C1s 54.9 at.% and 65.8 at.%, O1s 12.7 at.% and 16.1 at.% and Ag3d 32.3 at.% and 18.1 at.%, respectively. This last result is in accordance with the experimental evidence, reported above, of a different AgNPs concentration on the surface of the two samples. Examining the Ag3d doublet, as shown in Fig. 4b, it can be clearly seen that the two signals are mostly different. The Ag-1 curve is the one typical for metallic silver ($Ag^{(0)}$) [45], with very sharp peaks at 368.3 eV (Ag3d5/2) and 374.3 eV (Ag3d3/2) and a couple of satellite smaller peaks at about 372 and 378 eV, which are due to "loss features". These features are present only when Ag is in its metallic form, because they arise from the inelastic collision between the photoemitted

electrons from the 3d orbital, and the free delocalized electrons cloud, which is a fingerprint of a metallic state. Looking at the Ag-2 curve, it can be seen that the loss features are not present.

Moreover, the peaks are less sharp and highly asymmetric, which is due to the overlapping of two different oxidation states: one at lower binding energy (367.8 eV) due to Ag_2O [46], corresponding to 76.3% of the total amount of Ag, and another at higher binding energy (368.6 eV) due to metallic silver, corresponding to 23.7%. Thanks to the surface sensitivity of XPS technique, it could be assumed that the AgNPs on Ag-2 sample have a "core-shell" structure in which the outer part, the shell, is formed by Ag_2O, while the inner part, the core, is made up by $Ag^{(0)}$.

As already mentioned by Milošević et al. [25] the attenuation length in AgNPs is such that the signal arises only from the top 4 nm of the surface, with the majority of the signal belonging to the outermost 1.5 nm. This means that the Ag_2O outer layer is really thin, since it's possible to detect the $Ag^{(0)}$ signal from below. To have further confirmation about oxidation states, also the Modified Auger Parameters (MAP), which takes into account the relative position of the $Ag3d_{5/2}$ peak and the Ag MNN1 Auger peak, was checked. By a simple calculation [47], the following two values were obtained: 726.1 eV and 725.5 eV, for Ag-1 and Ag-2, respectively. The first value is typical for $Ag^{(0)}$, while the second one is in between $Ag^{(0)}$ reference value (726.1 eV) and Ag_2O reference value (724.4 eV). Since the MAP gives information related to the average oxidation state of the sample surface, these results confirm the mixture of oxidation state obtained from the deconvolution procedure (Fig. 5b). Thus, it can be affirmed that not only the morphological characteristics of the AgNPs deposited on Ag-1 and Ag-2 are different, but also the chemical composition of their outer part.

3.3.6 TGA analysis

The TGA thermograms of pristine PP mask, Ag-1 and Ag-2 are reported in the supplementary information (Fig. S3, Supporting Information). For all samples, the first decomposition stage occurred from room temperature to 150 °C indicating the removal of water and impurities. The second stage was observed between 180–450 °C for the pristine and Ag-2 mask and between 180-350 °C for Ag-1, attributed to the decomposition of the polymer. The residual mass of Ag-1 and Ag-2, 28% and 8%, respectively, correspond to the amount of AgNPs previously deposited on surgical masks, confirming the results obtained from SEM-EDX, XRD and XPS.

3.4 In vitro biocompatibility assessment

The possible cytotoxic effect of either pristine or silver-coated masks obtained by the sonication or agitation methods was evaluated by indirect contact assay according to ISO 10993-5 on L929 mouse fibroblasts or HaCaT human keratinocytes. Since human keratinocytes are the principal and most

abundant cells present in the epidermis, HaCaT have been chosen due to the direct and prolonged contact of surgical masks with the skin during wear [48]. The incubation of Ag-coated samples in the culture medium represent a more extreme environment with respect to the real contact between mask and skin. From the obtained results, no cytotoxic effect on either cell lines was observed with a cell viability higher than 70% for all tested samples (Fig. 5a). Uncoated surgical mask samples (spunbond PP layer) showed high biocompatibility, with average values of 86% for L929 cells, and 91% for HaCaT cells. The silver coatings obtained with either method slightly reduced the cell viability, but no significant differences were found compared to the uncoated masks. Both silver-coated samples are highly biocompatible towards human HaCaT cells proving that the AgNPs would not cause any harmful effect after contact with the skin during wear. SEM images of samples incubated 24 h in RPMI clearly show that the coatings are preserved (Fig. S4, Supporting Information). This further demonstrates that the SMR, which involves the reduction of Ag (I) ions to Ag metal and the oxidation of glucose into gluconic acid, which is non-toxic and biodegradable, does not produce harmful byproducts, making it safe for food and pharmaceutical applications.
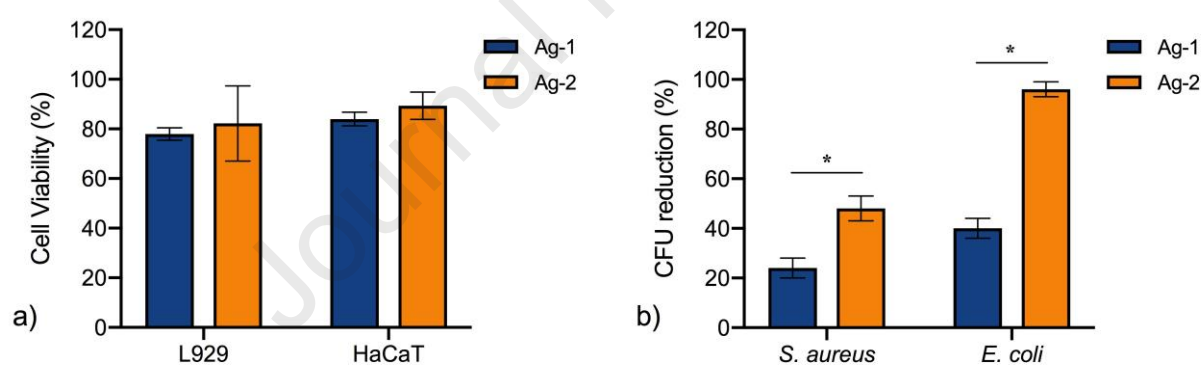

Figure 5. Biological characterization. (a) *In vitro* biocompatibility on L929 and HaCaT cells by indirect contact test evaluated by the MTT assay. Percentage of cell viability with respect to control groups (blanks). (b) Antibacterial activity vs *S. aureus* or *E. coli* calculated as the percentage reduction of CFU number with respect to the pristine PP surgical mask; * significance between bacterial strains within the same coating type (p < 0.0005). Results are expressed as mean ± SD calculated from at least three independent experiments.

3.5 Antibacterial activity assessment

The antibacterial activity of the proposed silver-coated surgical masks, Ag-1 and Ag-2, was analyzed by a direct contact test based on measuring the bacterial colony forming unit (CFU) number after their inoculation on the sample. *S. aureus* and *E. coli* were selected to perform the test. Specifically, the antibacterial efficacy was calculated as the percentage reduction of the bacterial CFU number

with respect to the pristine PP surgical mask. Fig. 5b shows that both silver coatings exerted a relevant antibacterial activity reducing both *S. aureus* and *E. coli* viability. In particular, Ag-1 caused a CFU number reduction of around 24% and 40% of *S. aureus* and *E. coli*, respectively, whereas the decrease of *S. aureus* and *E. coli* CFU exerted by Ag-2 was around 48% and 96%, respectively.

According to the literature [49][50], these results demonstrate a higher antibacterial efficacy of both silver coatings versus *E. coli* compared with *S. aureus*. Martinez-Castanon et al. demonstrated that the minimum inhibition concentration of AgNPs with different sizes for all tested samples is lower against *E. coli* than against *S. aureus* [50]. More comparisons are presented in Table S1 (Supporting Information).

The Ag-2 sample was characterized by a double percentage reduction of both bacterial CFU with respect to Ag-1. As reported by Zheng et al. [12], one of the most important aspects in determining biological function and interaction with cells of AgNPs is their size. At same doses, smaller size NPs (e.g., 5 nm in diameter) have greater surface-area-to-volume ratio which improves their interaction with bacteria, determining higher antimicrobial efficiency as well as faster bacterial killing behavior [12]. In addition, the shape of AgNPs could directly influence the interactions with the bacterial membrane [12][14][51].

As discussed above, the different antibacterial properties of Ag-1 and Ag-2 are probably related to the characteristics of the coatings, since AgNPs in Ag-1 are fused together, decreasing the surface-area-to-volume ratio, whereas in Ag-2 individual AgNPs homogenously coat the microfibers surface.


3.6   Antiviral properties assessment

Antiviral properties of Ag-1 and Ag-2 silver masks were performed against SARS-CoV-2 after 1, 5, 10, 30, and 60 minutes of contact. The results of virus inhibition are reported in Table 1. The Ag-2 coating showed better antiviral properties than Ag-1 at earlier time points. In fact, at 1 minute of contact with the SARS-CoV-2, the Ag-2 silver-coated mask had an antiviral capacity of 75% against 24% of the Ag-1 and 90% against 68% at 5 minutes. For longer contact times no differences were observed between samples and both achieved 100% of viral inhibition at 60 minutes.

Table 1. Antiviral properties of pristine surgical mask (untreated PP) and with Ag-1 and Ag-2 coatings at different timepoints.

	Viral inhibition (%)					
Time points	**0**	**1**	**5**	**10**	**30**	**60**
Polypropylene	0	1	1	0	0	24

| Ag-1 | 0 | 24 | 68 | 93 | 99 | 100 |
| Ag-2 | 0 | 75 | 90 | 92 | 95 | 100 |
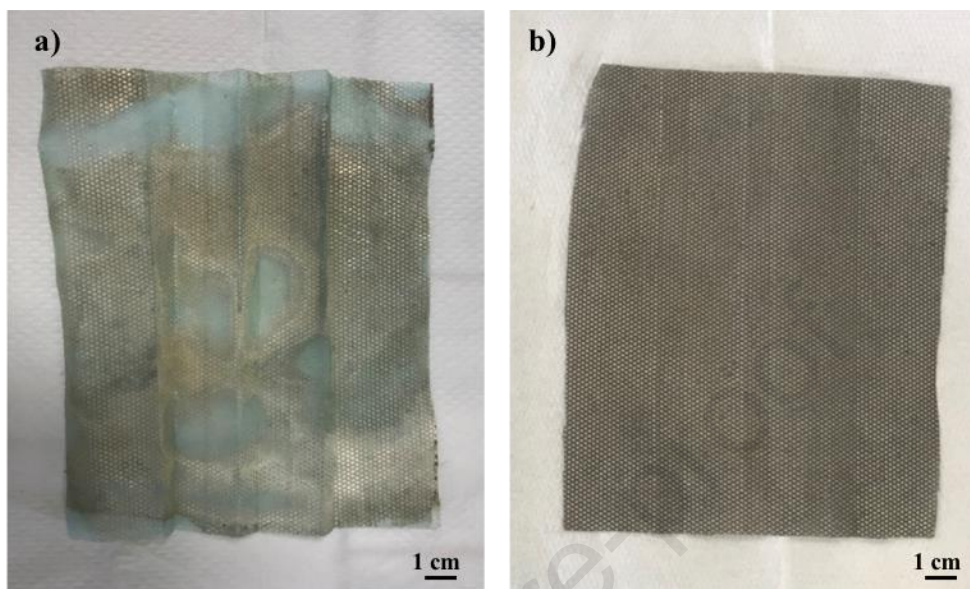
Baselga et al. proposed a silver nanoparticles-polyethyleneimine-based coating on surgical masks showing a viral load reduction of 98% after 10 min of contact while the 99.9% was reached after 2 h of infection [23]. The Ag-2 coating proposed in this study showed comparable results. More comparisons are presented in Table S1 (Supporting Information).

3.7 Scalability

The two SMR coating reactions were also applied to real-sized samples (about 15 x 12 cm). The Ag-1 coating obtained by sonication appeared extremely nonhomogeneus and even absent in some areas (Fig. 6a). This was probably related to non-uniformly distributed cavitation intensities in the ultrasonic bath [52]. Contrarily, the Ag-2 coating had no scale-up drawbacks and was homogenous throughout the entire surface (Fig 6b). Despite the biocompatibility and antimicrobial properties of Ag-1, the non-scalability limits the application of SMR and sonication method for the development of antimicrobial real-sized surgical mask. Therefore, the mechanical testing, BFE and breathability were investigated only for Ag-2 samples.

Figure 6. Real-sized spunbond polypropylene surgical mask silver-coated by *in situ* silver mirror reaction (SMR) combined with (a) sonication or (b) agitation methods; scale bar 1 cm.

3.7.1 Mechanical characterization

The mechanical characterization aimed at comparing the properties of Ag-coated and pristine masks, and qualitatively evaluating the adhesion of AgNPs on PP fibers. The tensile test was performed only on Ag-2 sample due to the better uniformity of the silver coating. The failure mechanisms of PP spunbond involve various factors, such as the progressive untangling and reorientation of the PP microfibers, the presence of welding points, or the microfibers plastic deformation in the direction of the load [53]. The stress-strain curves of Ag-2 and PP had identical profiles (Fig. S5, Supporting Information). Both curves presented an initial linear section and a subsequent non-linear section which continued up to the point of maximum stress; after this point, a reduction of the load-bearing capacity was observed for both samples (not shown in the curve). The elastic moduli of pristine PP and Ag-2 were highly comparable and equal to 38 MPa, consistently with other results found in the literature [6][54]. Although the Ag-coating procedure had no effect on the strength of PP, it appeared to reduce its elongation capacity and, overall, its ductility; for instance, the elongation at break decreased from 53% for PP to 35% for Ag-2 (Fig. S5, Supporting Information). The breaking takes place in a fairly localized area, which undergoes a necking phenomenon, where the microfibers progressively unravel and align with the load direction, up to the formation of a single filament; outside this area, the sample does not appear significantly damaged. The color of the microfibers of Ag-2 remained grey, even at the breaking point where the PP microfibers are macroscopically frayed. Moreover, SEM analysis showed that around the breaking point, PP microfibers were plastically deformed, and AgNPs were still deposited on them, although no longer homogeneously coated their surface (Fig. S6, Supporting Information). This suggests that the physical adsorption of AgNPs, occurring on PP fibers during the coating, provides their strong adhesion on the microfibers' surface.

3.7.2 Functional tests of Personal Protective Equipment

The BFE and breathability of pristine and Ag-2 masks were measured according to UNI EN 14683:2019. The preservation of these two characteristics is essential to ensure the correct functioning of surgical masks and users' comfort. Due to the thin and homogeneous Ag-coating on the spunbond PP fibers, which presented very few clusters, no significant alterations of these two parameters were observed with respect to the untreated mask. Specifically, the breathability of masks with the Ag-2 outer layer was around 5.3 Pa/cm^2, largely below the 40 Pa/cm^2 threshold value for type I and type II face masks. Regarding the BFE results, the Ag coating caused a reduction of the

filtration ability around 5%. Therefore, the proposed Ag-2 mask is suitable to be used as a commercial single use surgical mask with improved antimicrobial properties.

4 Conclusions

Two silver-coated polypropylene surgical masks, Ag-1 and Ag-2, were obtained using the Silver Mirror Reaction through sonication and agitation methods, respectively, with a simple one-step approach. The Ag-2 sample was characterized by individual AgNPs (~150 nm) uniformly coating PP microfibers, whereas in Ag-1 AgNPs were fused together, forming a continuous and dense layer. Both coatings possessed significant biological properties, such as biocompatibility on human keratinocytes, antibacterial activity versus *E. coli* and *S. aureus*, and antiviral action versus SARS-CoV-2. Nonetheless, only the SMR combined with agitation was scalable to real-size samples. The SMR is simple and reproducible, requires few reagents, mild temperatures, short reaction times and no expensive equipment are required, resulting in a scalable method for industrial applications. Based on the obtained results, the SMR combined with agitation could be applied for the functionalization of other fabric substrates to develop antibacterial and antiviral personal protective equipment, especially for medical facilities. Further investigations could be performed to optimize the concentration of $AgNO_3$ used in the SMR solution and reduce the coating costs.

Conflict of interest

All authors have no conflict of interest

Authors contribution

Conceptualization, I.V.F., A.Cat., and P.L.; **Methodology**, I.V.F., G.G., A.P., A.Cav., R.F., A.R., T.AK., R.M., A.V., M.C., and S.A.; **Data curation**, I.V.F., G.G., A.P., R.M. and M.C.; **Writing—original draft**, I.V.F., G.G., A.P., A.Cav., P.M., R.M., and M.C; **Writing—review & editing**, I.V.F., G.G., A.P., A.Cav., P.M., A.Cat., and P.L.; **Supervision**, P.L.; **Funding acquisition**, P.L. and G.S. All authors have read and agreed to the published version of the manuscript.

Data availability statement

Data associated with this study have not been deposited into a publicly available repository, and are included in the article/supplementary material or are referenced in the article.

References

[1] S.E. Eikenberry, M. Mancuso, E. Iboi, T. Phan, K. Eikenberry, Y. Kuang, E. Kostelich, A.B. Gumel, To mask or not to mask: Modeling the potential for face mask use by the general public to curtail the COVID-19 pandemic, Infect. Dis. Model. 5 (2020) 293–308. https://doi.org/10.1016/j.idm.2020.04.001.

[2] M. Liao, H. Liu, X. Wang, X. Hu, Y. Huang, X. Liu, K. Brenan, J. Mecha, M. Nirmalan, J.R. Lu, A technical review of face mask wearing in preventing respiratory COVID-19 transmission, Curr. Opin. Colloid Interface Sci. 52 (2021) 293. https://doi.org/10.1016/j.cocis.2021.101417.

[3] J. Howard, A. Huang, Z. Li, Z. Tufekci, V. Zdimal, H.M. van der Westhuizen, A. von Delft, A. Price, L. Fridman, L.H. Tang, V. Tang, G.L. Watson, C.E. Bax, R. Shaikh, F. Questier, D. Hernandez, L.F. Chu, C.M. Ramirez, A.W. Rimoin, An evidence review of face masks against COVID-19, Proc. Natl. Acad. Sci. U. S. A. 118 (2021). https://doi.org/10.1073/pnas.2014564118.

[4] A. Tcharkhtchi, N. Abbasnezhad, M. Zarbini Seydani, N. Zirak, S. Farzaneh, M. Shirinbayan, An overview of filtration efficiency through the masks: Mechanisms of the aerosols penetration, Bioact. Mater. 6 (2021) 106–122. https://doi.org/10.1016/j.bioactmat.2020.08.002.

[5] S. Arora, A. Majumdar, Face masks to fight against COVID-19 pandemics: A comprehensive review of materials, design, technology and product development, J. Ind. Text. 51 (2022) 3613S-3647S. https://doi.org/10.1177/15280837211069869.

[6] V. Varanges, B. Caglar, Y. Lebaupin, T. Batt, W. He, J. Wang, R.M. Rossi, G. Richner, J.R. Delaloye, V. Michaud, On the durability of surgical masks after simulated handling and wear, Sci. Rep. 12 (2022) 1–10. https://doi.org/10.1038/s41598-022-09068-1.

[7] W. Deng, Y. Sun, X. Yao, K. Subramanian, C. Ling, H. Wang, S.S. Chopra, B. Bin Xu, J.X. Wang, J.F. Chen, D. Wang, H. Amancio, S. Pramana, R. Ye, S. Wang, Masks for COVID-19, Adv. Sci. 9 (2022) 2102189. https://doi.org/10.1002/advs.202102189.

[8] B. Atılgan Türkmen, Life cycle environmental impacts of disposable medical masks,

Environ. Sci. Pollut. Res. 29 (2022) 25496–25506. https://doi.org/10.1007/s11356-021-17430-5.

[9] L. De Sio, B. Ding, M. Focsan, K. Kogermann, P. Pascoal-Faria, F. Petronela, G. Mitchell, E. Zussman, F. Pierini, Personalized Reusable Face Masks with Smart Nano-Assisted Destruction of Pathogens for COVID-19: A Visionary Road, Chem. - A Eur. J. 27 (2021) 6112–6130. https://doi.org/10.1002/chem.202004875.

[10] A. Gonzalez, H.A. Aboubakr, J. Brockgreitens, W. Hao, Y. Wang, S.M. Goyal, A. Abbas, Durable nanocomposite face masks with high particulate filtration and rapid inactivation of coronaviruses, Sci. Rep. 11 (2021). https://doi.org/10.1038/s41598-021-03771-1.

[11] T. Hamouda, H. Kafafy, H.M. Mashaly, N.M. Aly, Breathability performance of antiviral cloth masks treated with silver nanoparticles for protection against COVID-19, J. Ind. Text. 51 (2022) 1494–1523. https://doi.org/10.1177/15280837211051100.

[12] K. Zheng, M.I. Setyawati, D.T. Leong, J. Xie, Antimicrobial silver nanomaterials, Coord. Chem. Rev. 357 (2018) 1–17. https://doi.org/10.1016/j.ccr.2017.11.019.

[13] I. Ijaz, A. Bukhari, E. Gilani, A. Nazir, H. Zain, R. Saeed, S. Hussain, T. Hussain, A. Bukhari, Y. Naseer, R. Aftab, Green synthesis of silver nanoparticles using different plants parts and biological organisms, characterization and antibacterial activity, Environ. Nanotechnology, Monit. Manag. 18 (2022) 100704. https://doi.org/10.1016/j.enmm.2022.100704.

[14] S. Chernousova, M. Epple, Silver as antibacterial agent: Ion, nanoparticle, and metal, Angew. Chemie - Int. Ed. 52 (2013) 1636–1653. https://doi.org/10.1002/anie.201205923.

[15] F. Pilaquinga, R. Bosch, J. Morey, C. Bastidas-Caldes, M. Torres, F. Toscano, A. Debut, K. Pazmiño-Viteri, M. de las Nieves Piña, High in vitro activity of gold and silver nanoparticles from Solanum mammosum L. against SARS-CoV-2 surrogate Phi6 and viral model PhiX174, Nanotechnology. 34 (2023). https://doi.org/10.1088/1361-6528/acb558.

[16] M. Rehan, H.M. Mashaly, S. Mowafi, A. Abou El-Kheir, H.E. Emam, Multi-functional textile design using in-situ Ag NPs incorporation into natural fabric matrix, Dye. Pigment. 118 (2015) 9–17. https://doi.org/10.1016/j.dyepig.2015.02.021.

[17] P. Merkl, S. Long, G.M. McInerney, G.A. Sotiriou, Antiviral Activity of Silver, Copper Oxide and Zinc Oxide Nanoparticle Coatings against SARS-CoV-2, Nanomaterials. 11 (2021). https://doi.org/10.3390/nano11051312.

[18] A.K. Chatterjee, R. Chakraborty, T. Basu, Mechanism of antibacterial activity of copper nanoparticles, Nanotechnology. 25 (2014). https://doi.org/10.1088/0957-4484/25/13/135101.

[19] G. Grass, C. Rensing, M. Solioz, Metallic copper as an antimicrobial surface, Appl. Environ. Microbiol. 77 (2011) 1541–1547. https://doi.org/10.1128/AEM.02766-10.

[20] D. Reinhold, S. Brocke, The differential roles of zinc in immune responses and their potential implications in antiviral immunity against SARS-CoV-2, Clin. Nutr. 40 (2021) 652. https://doi.org/10.1016/j.clnu.2020.12.005.

[21] C.B. Hiragond, A.S. Kshirsagar, V. V. Dhapte, T. Khanna, P. Joshi, P. V. More, Enhanced anti-microbial response of commercial face mask using colloidal silver nanoparticles, Vacuum. 156 (2018) 475–482. https://doi.org/10.1016/j.vacuum.2018.08.007.

[22] C. Rigo, L. Ferroni, I. Tocco, M. Roman, I. Munivrana, C. Gardin, W.R.L. Cairns, V. Vindigni, B. Azzena, C. Barbante, B. Zavan, Active silver nanoparticles for wound healing,

Int. J. Mol. Sci. 14 (2013) 4817–4840. https://doi.org/10.3390/ijms14034817.

[23] M. Baselga, I. Uranga-Murillo, D. de Miguel, M. Arias, V. Sebastián, J. Pardo, M. Arruebo, Silver Nanoparticles–Polyethyleneimine-Based Coatings with Antiviral Activity against SARS-CoV-2: A New Method to Functionalize Filtration Media, Materials (Basel). 15 (2022). https://doi.org/10.3390/ma15144742.

[24] S. Iravani, H. Korbekandi, S. V. Mirmohammadi, B. Zolfaghari, Synthesis of silver nanoparticles: chemical, physical and biological methods, Res. Pharm. Sci. 9 (2014) 385–406. http://www.ncbi.nlm.nih.gov/pubmed/26339255%0Ahttp://www.pubmedcentral.nih.gov/articlerender.fcgi?artid=PMC4326978.

[25] M. Milošević, M. Radoičić, Z. Šaponjić, T. Nunney, D. Marković, J. Nedeljković, M. Radetić, In situ generation of Ag nanoparticles on polyester fabrics by photoreduction using TiO2 nanoparticles, J. Mater. Sci. 48 (2013) 5447–5455. https://doi.org/10.1007/s10853-013-7338-1.

[26] F. Seidi, C. Deng, Y. Zhong, Y. Liu, Y. Huang, C. Li, H. Xiao, Functionalized Masks: Powerful Materials against COVID-19 and Future Pandemics, Small. 17 (2021) 2102453. https://doi.org/10.1002/smll.202102453.

[27] P. Naksen, P. Jarujamrus, W. Anutrasakda, V. Promarak, L. Zhang, W. Shen, Old silver mirror in qualitative analysis with new shoots in quantification: Nitrogen-doped carbon dots (N-CDs) as fluorescent probes for "off-on" sensing of formalin in food samples, Talanta. 236 (2022) 122862. https://doi.org/10.1016/j.talanta.2021.122862.

[28] W.E. Benet, G.S. Lewis, L.Z. Yang, D.E. Peter Hughes, The mechanism of the reaction of the Tollens reagent, J. Chem. Res. 35 (2011) 675–677. https://doi.org/10.3184/174751911X13206824040536.

[29] L. Qu, L. Dai, Novel silver nanostructures from silver mirror reaction on reactive substrates, J. Phys. Chem. B. 109 (2005) 13985–13990. https://doi.org/10.1021/jp0515838.

[30] Y. Saito, J.J. Wang, D.N. Batchelder, D.A. Smith, Simple Chemical Method for Forming Silver Surfaces with Controlled Grain Sizes for Surface Plasmon Experiments, Langmuir. 19 (2003) 6857–6861.

[31] Z. Shan, J. Wu, F. Xu, F.Q. Huang, H. Ding, Highly effective silver/semiconductor photocatalytic composites prepared by a silver mirror reaction, J. Phys. Chem. C. 112 (2008) 15423–15428. https://doi.org/10.1021/jp804482k.

[32] Q. Huang, K. Zhang, Y. Yang, J. Ren, R. Sun, F. Huang, X. Wang, Highly smooth, stable and reflective Ag-paper electrode enabled by silver mirror reaction for organic optoelectronics, Chem. Eng. J. 370 (2019) 1048–1056. https://doi.org/10.1016/J.CEJ.2019.03.258.

[33] L. Hu, Z. Kang, Enhanced flexible polypropylene fabric with silver/magnetic carbon nanotubes coatings for electromagnetic interference shielding, Appl. Surf. Sci. 568 (2021) 150845. https://doi.org/10.1016/j.apsusc.2021.150845.

[34] V.A. Zhukovskii, T.Y. Anushchenko, D. Tagandurdyeva, V.A. Khokhlova, Preparation and Study of Polymer Implants with a Silver Nanocoating, Fibre Chem. 50 (2018) 264–269. https://doi.org/10.1007/s10692-019-09973-8.

[35] Q. Liao, D. Chen, X. Zhang, Y. Ma, B. Yang, C. Zhao, W. Yang, Surface Engineering of Organic Polymers by Photo-induced Free Radical Coupling with p-Dimethylaminophenyl

Group as A Synthesis Block, ChemistrySelect. 5 (2020) 3365–3373.
https://doi.org/10.1002/slct.202000082.

[36] Z. Wang, J. Ou, Y. Wang, M. Xue, F. Wang, B. Pan, C. Li, W. Li, Anti-bacterial
      superhydrophobic silver on diverse substrates based on the mussel-inspired polydopamine,
      Surf. Coatings Technol. 280 (2015) 378–383. https://doi.org/10.1016/j.surfcoat.2015.09.023.

[37] M. Zhang, M. Wang, M. Zhang, C. Yang, Y. Li, Y. Zhang, J. Hu, G. Wu, Flexible and
      Thermally Induced Switchable Fire Alarm Fabric Based on Layer-by-Layer Self-Assembled
      Silver Sheet/Fe3O4 Nanowire Composite, ACS Appl. Mater. Interfaces. 11 (2019) 47456–
      47467. https://doi.org/10.1021/acsami.9b18858.

[38] ICCD, The International Centre for Diffraction Data, (2012). https://www.icdd.com/
      (accessed May 15, 2023).

[39] E. Briganti, T. Al Kayal, S. Kull, P. Losi, D. Spiller, S. Tonlorenzi, D. Berti, G. Soldani, The
      effect of gamma irradiation on physical-mechanical properties and cytotoxicity of
      polyurethane-polydimethylsiloxane microfibrillar vascular grafts, J. Mater. Sci. Mater. Med.
      21 (2010) 1311–1319. https://doi.org/10.1007/s10856-009-3943-6.

[40] I. Foffa, P. Losi, P. Quaranta, A. Cara, T. Al Kayal, M. D'Acunto, G. Presciuttini, M.
      Pistello, G. Soldani, A Copper nanoparticles-based polymeric spray coating: Nanoshield
      against Sars-Cov-2, J. Appl. Biomater. Funct. Mater. 20 (2022) 228080002210763.
      https://doi.org/10.1177/22808000221076326.

[41] P. Quaranta, G. Lottini, G. Chesi, F. Contrafatto, R. Russotto, L. Macera, M. Lai, P.G.
      Spezia, A. Brai, M. Botta, G. Freer, M. Pistello, DDX3 inhibitors show antiviral activity
      against positive-sense single-stranded RNA viruses but not against negative-sense single-
      stranded RNA viruses: The coxsackie B model, Antiviral Res. 178 (2020) 104750.
      https://doi.org/10.1016/j.antiviral.2020.104750.

[42] S.K. Nemani, R.K. Annavarapu, B. Mohammadian, A. Raiyan, J. Heil, M.A. Haque, A.
      Abdelaal, H. Sojoudi, Surface Modification of Polymers: Methods and Applications, Adv.
      Mater. Interfaces. 5 (2018) 1801247. https://doi.org/10.1002/admi.201801247.

[43] M. Abulikemu, B.E.A. Tabrizi, S.M. Ghobadloo, H.M. Mofarah, G.E. Jabbour, Silver
      Nanoparticle-Decorated Personal Protective Equipment for Inhibiting Human Coronavirus
      Infectivity, ACS Appl. Nano Mater. 5 (2022) 309–317.
      https://doi.org/10.1021/acsanm.1c03033.

[44] K. AbdelRahim, S.Y. Mahmoud, A.M. Ali, K.S. Almaary, A.E.Z.M.A. Mustafa, S.M.
      Husseiny, Extracellular biosynthesis of silver nanoparticles using Rhizopus stolonifer, Saudi
      J. Biol. Sci. 24 (2017) 208–216. https://doi.org/10.1016/j.sjbs.2016.02.025.

[45] A.M. Ferraria, A.P. Carapeto, A.M. Botelho Do Rego, X-ray photoelectron spectroscopy:
      Silver salts revisited, Vacuum. 86 (2012) 1988–1991.
      https://doi.org/10.1016/j.vacuum.2012.05.031.

[46] K. Rajan, A. Chiappone, D. Perrone, S. Bocchini, I. Roppolo, K. Bejtka, M. Castellino, C.F.
      Pirri, C. Ricciardi, A. Chiolerio, Ionic liquid-enhanced soft resistive switching devices, RSC
      Adv. 6 (2016) 94128–94138. https://doi.org/10.1039/c6ra18668h.

[47] C.D. Wagner, The NIST X-Ray Photoelectron Spectroscopy (XPS) Database, (1991).
      https://doi.org/10.6028/NIST.TN.1289.

[48] S. Alarifi, D. Ali, A. Verma, S. Alakhtani, B.A. Ali, Cytotoxicity and genotoxicity of copper
      oxide nanoparticles in human skin keratinocytes cells, Int. J. Toxicol. 32 (2013) 296–307.

https://doi.org/10.1177/1091581813487563.

[49] I. Maliszewska, Z. Sadowski, Synthesis and antibacterial activity of of silver nanoparticles, J. Phys. Conf. Ser. 146 (2009). https://doi.org/10.1088/1742-6596/146/1/012024.

[50] G.A. Martínez-Castañón, N. Niño-Martínez, F. Martínez-Gutierrez, J.R. Martínez-Mendoza, F. Ruiz, Synthesis and antibacterial activity of silver nanoparticles with different sizes, J. Nanoparticle Res. 10 (2008) 1343–1348. https://doi.org/10.1007/s11051-008-9428-6.

[51] X. Wang, Y. Du, L. Fan, H. Liu, Y. Hu, Chitosan- metal complexes as antimicrobial agent: Synthesis, characterization and Structure-activity study, Polym. Bull. 55 (2005) 105–113. https://doi.org/10.1007/s00289-005-0414-1.

[52] C. Agarkoti, P.R. Gogate, Mapping of cavitation intensity in a novel dual-frequency ultrasonic reactor of capacity 10 L, Chem. Eng. Sci. 259 (2022) 117833. https://doi.org/10.1016/j.ces.2022.117833.

[53] R. Jubera, A. Ridruejo, C. González, J. Llorca, Mechanical behavior and deformation micromechanisms of polypropylene nonwoven fabrics as a function of temperature and strain rate, Mech. Mater. 74 (2014) 14–25. https://doi.org/10.1016/j.mechmat.2014.03.007.

[54] S. Kilmartin-Lynch, M. Saberian, J. Li, R. Roychand, G. Zhang, Preliminary evaluation of the feasibility of using polypropylene fibres from COVID-19 single-use face masks to improve the mechanical properties of concrete, J. Clean. Prod. 296 (2021) 126460. https://doi.org/10.1016/j.jclepro.2021.126460.

Declaration of interests

☒ The authors declare that they have no known competing financial interests or personal relationships that could have appeared to influence the work reported in this paper.

☐ The authors declare the following financial interests/personal relationships which may be considered as potential competing interests: